

Combining Visual Saliency Methods and Sparse Keypoint Annotations to Providently Detect Vehicles at Night

Lukas Ewecker,^{*,1} Lars Ohnemus,^{*,2} Robin Schwager,^{*,1} Stefan Roos,¹ and Sascha Saralajew^{*,3}

Abstract—Provident detection of other road users at night has the potential for increasing road safety. For this purpose, humans intuitively use visual cues, such as light cones and light reflections emitted by other road users to be able to react to oncoming traffic at an early stage. This behavior can be imitated by computer vision methods by predicting the appearance of vehicles based on emitted light reflections caused by the vehicle’s headlights. Since current object detection algorithms are mainly based on detecting directly visible objects annotated via bounding boxes, the detection and annotation of light reflections without sharp boundaries is challenging. For this reason, the extensive open-source dataset PVDN (Provident Vehicle Detection at Night) was published, which includes traffic scenarios at night with light reflections annotated via keypoints. In this paper, we explore the potential of saliency-based approaches to create different object representations based on the visual saliency and sparse keypoint annotations of the PVDN dataset. For that, we extend the general idea of Boolean map saliency towards a context-aware approach by taking into consideration sparse keypoint annotations by humans. We show that this approach allows for an automated derivation of different object representations, such as binary maps or bounding boxes so that detection models can be trained on different annotation variants and the problem of providently detecting vehicles at night can be tackled from different perspectives. With that, we provide further powerful tools and methods to study the problem of detecting vehicles at night before they are actually visible.

I. INTRODUCTION

Current State-Of-The-Art (SOTA) methods in object detection mostly rely on annotations via bounding boxes. This is a valid approach as objects commonly considered in such tasks are easily describable by bounding boxes. A car, for example, has very clear and objectively definable object borders. This makes it very easy for human annotators to draw a bounding box around a car, as they have no problem identifying the car’s boundaries. However, objectively drawing bounding boxes becomes a challenge when dealing with objects that are not described by clear, sharp boundaries. When an object seemingly fades into the background, it is difficult to set rules for manual annotation. This ultimately leads to a high degree of uncertainty in the annotations of different annotators and can result in highly variable

annotations. This phenomenon becomes evident when dealing with the problem of predictive vehicle detection at night. The problem was first brought up by Oldenziel et al. [1] and recently Saralajew et al. [2] published a corresponding large-scale dataset called PVDN dataset, where oncoming vehicles and their corresponding light reflections are annotated. Here, the objective labeling of light reflections with a fuzzy nature and its soft borders emerged as a problem. To this end, they conducted a study comparing the consistency of different annotators via bounding boxes for the same images. They conclude that the expert annotators could not agree on a consistent ground truth, which can cause problems for systems learning from this data. Consequently, the dataset was not annotated using bounding boxes but instead using keypoints placed on the point with the highest intensity of each light instance. This allows for a much more objective annotation and leaves room to automatically derive rule-based object representations, such as bounding boxes. Saralajew et al. [2] already mentioned the possibility of using saliency-based approaches in order to objectively derive saliency maps from the keypoint annotations and use them to generate different object representations, such as binary maps or bounding boxes. Visual saliency thereby is the perceptual quality that makes certain objects in images “stand out” from their surroundings and thus attract human attention.

In this paper, we study the potential of saliency-based approaches in order to detect oncoming vehicles at night. We show how to automatically derive various object representations based on visual saliency and given the sparse keypoint annotations of the PVDN dataset, such as bounding boxes as well as binary masks. Also, we analyze the advantages and limitations of this method and show that visual saliency is a suitable approach to annotate objects with fuzzy borders objectively. With that contribution, we want to provide further tools and methods to work with the PVDN dataset and enable fellow researchers to study the problem of providently detecting vehicles at night. For that, we also publish the source code for the proposed method.⁴

The paper is organized as follows. First, we provide a brief overview of the related work on the topics of visual saliency and provident vehicle detection at night. Second, we explain the proposed saliency method. After that, we give a short excursion to other possible application areas for the proposed method, followed by experiments that use the proposed approach to phrase the task of provident vehicle detection at night both as an object detection and a semantic

^{*}Authors contributed equally.

¹Dr. Ing. h.c. F. Porsche AG, Weissach, Germany. {lukas.ewecker, robin.schwager, stefan.roos4}@porsche.de

²Karlsruhe Institute of Technology (KIT), Germany. The research was performed during employment at Dr. Ing. h.c. F. Porsche AG. lars.ohnemus@student.kit.edu

³NEC Laboratories Europe GmbH, Heidelberg, and Leibniz University Hannover, Institute of Product Development, Hannover, both Germany. The research was performed during employment at Dr. Ing. h.c. F. Porsche AG. sascha.saralajew@neclab.eu

⁴<https://github.com/lukazso/kpbms-pvdn/>

segmentation problem. We finish the paper with a conclusion and outlook towards future work.

II. RELATED WORK

Saliency detection is an active field of research, despite its long history [3]. There are many different approaches to mimic the human attention mechanism. For example, Itti et al. [4] presented a model of human attention which uses three different feature maps—color, orientation, and intensity—and center-surround mechanisms at different scales to generate saliency maps [4], [5]. Newer research focuses both on conventional computer vision (e. g., [6], [7]) as well as deep learning approaches (e. g., [8], [9], [10]) to generate saliency maps and to detect salient objects. Saliency maps can be used for various applications in the field of computer vision [3]. Most prominently, saliency maps can be used to infer segmentation masks for salient object segmentation as well as classify salient objects [11]. Other use cases are visual tracking and video compression [3]. Visual saliency can also be applied in the automotive context to mimic the human perception apparatus [12], [13]. Pugeault and Bowden [14] investigated how much of human behavior during driving happens preattentive—and therefore at a more fundamental level in the human visual perception. They also showed that current bottom-up saliency methods are not expressive enough to be successfully used in the automotive context. Human superiority suggests potential for elaborating better models of human perception. This discrepancy is even more visible at night when visual perception is even more difficult.

At night, the human provident, preattentive behavior is still unchallenged by advanced driver assistance systems, which are currently mostly relying on visible headlights of other cars to detect them [15], [16], [17], [18], [19], [20]. Therefore, early signs of oncoming vehicles like local light reflections on guardrails and the street are unused features that humans highly rely on. Oldenziel et al. [1] studied the deficit between human provident vehicle detection and a camera-based vehicle detection system. Based on a test group study, they showed that drivers detected oncoming vehicles on average 1.7 s before the camera system, which is a not negligible time discrepancy. Tests showed that deep learning predictors can detect oncoming vehicles based on light artifacts to some extent [1], [2]. In their analysis, they raised concerns about the ability to describe fuzzy light artifacts through rigid bounding boxes used in the evaluated predictors [2]. As a consequence, Saralajew et al. [2] published the PVDN dataset containing around 60 000 annotated gray-scale images. There, all *light instances* (light artifacts) caused by oncoming vehicles are annotated. Those light instances are categorized in *direct* (e. g., headlights) and *indirect* (e. g., light reflections on guardrails caused by the oncoming vehicle) instances. In contrast to Oldenziel et al. [1], the PVDN dataset uses keypoint annotations which capture human attention through a clear annotation hierarchy to allow the investigation of several use cases, for example, regressing more objective bounding box representations. Moreover, with the keypoints as initial seeds, the authors further explored methods to extend the

keypoint annotations to bounding boxes with low annotation uncertainty and successfully trained both shallow and deep learners on the regressed annotations. The bounding box regression in their work is based on a simple thresholding schema [2]. They also addressed the possibility of combining their sparse keypoint annotations with visual saliency methods to enhance the information content of the PVDN data. This work picks this idea up and provides a simple tool to extend the base keypoint annotations.

III. ATTENTION GENERATION METHOD

Visual saliency offers a mechanism to extract pertinent regions of interest from images. This attention is based purely on the local topography and is not biased towards a specific problem. However, when combined with a sparse human annotation, the salient regions can be filtered to assert context upon the resulting saliency maps. These maps then provide more information than both methods alone could. This emergence is exploited by the problem-aware attention generation method that we propose. This section introduces the method and specifies an algorithm based on the robust Boolean Map Saliency (BMS) method to generate context-aware attention maps.

A. Baseline Saliency Detection

Saliency detection is a well-studied task. A simple and effective method to detect saliency is to use human perception mechanisms, for example, figure-ground segregation. One factor likely influencing this segregation is the surroundedness of salient objects by background. Zhang and Sclaroff [6] formulated the BMS method around this relationship. Their method applies randomly sampled thresholding to an image, generating so-called Boolean maps. These Boolean maps are hypothesized to characterize the image and its salient regions [21]. Using binary image processing techniques, surrounded contours are activated. The attention and thus saliency is then computed by averaging the activated Boolean maps [21]. The activation is performed by masking regions in the Boolean map that are connected to the image's borders [21]. The BMS method is used as a baseline saliency generator for our compound approach, as its topographic nature allows the combination with sparse keypoint annotations, which are essential for the proposed method. The adaption relies on a different formulation of the Boolean map generation. Instead of only using the raw image data as information, a sparse set of fixture points (keypoints) is provided through annotation. These points are located in regions that the human annotator judges interesting for a specific problem. An example of this annotation technique was used by Saralajew et al. [2] in the PVDN dataset. The generation of saliency maps can then be performed as a data augmentation step. Using the fixture points, the figure-ground segregation can be rephrased: A region is considered salient if it surrounds a fixture point. In the following paragraphs, a similar nomenclature and workflow to Zhang and Sclaroff [21] is presented for easy comparison. Fig. 1 shows both methods side-by-side.

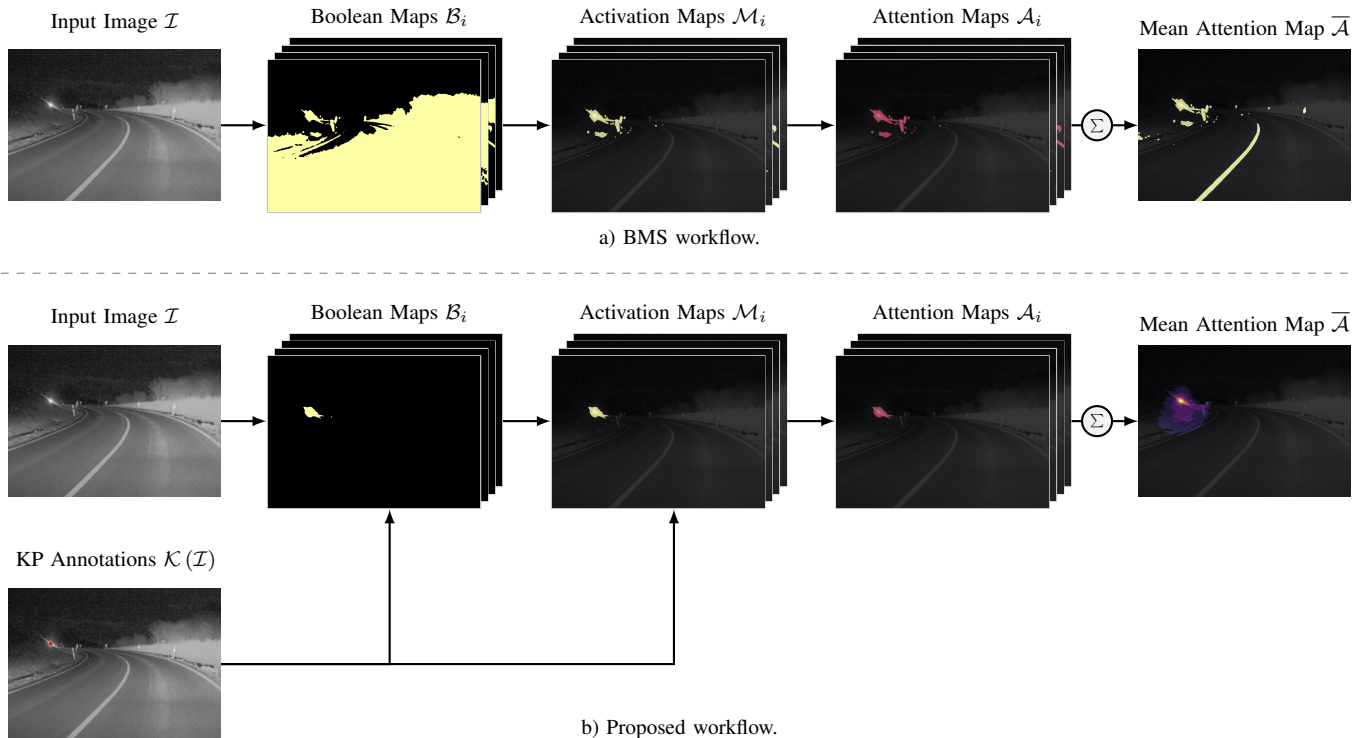


Fig. 1. Comparison of the different pipelines: The upper part shows the pipeline of the original BMS method [21] for reference, while the lower part shows the adapted pipeline (our method). The example image used is from the PVDN dataset (ID: 017358, [2]).

B. Boolean Map Generation

The generation of Boolean maps \mathcal{B}_i is performed analogously to Zhang and Sclaroff [6] by randomly thresholding the input image’s feature maps $\phi(\mathcal{I})$ at the threshold θ_i :

$$\mathcal{B}_i = \text{THRESH}(\phi(\mathcal{I}), \theta_i). \quad (1)$$

For the studied dataset, only one feature map has to be considered, as all images are grayscale. However, the proposed method is also extendable to multi-channel images. A color transformation as applied in the original BMS method is omitted for simplicity. For applications with multi-channel images, this step can be added. Using the keypoint’s intensity, the number of sampled thresholds can also be reduced. Per definition, thresholds higher than the keypoint’s intensity have no significant effect on the regions saliency. Also, low thresholds can be ignored to speed-up the computation process. Therefore, the threshold θ_i can be sampled from a uniform distribution around the intensity value $\phi(\mathcal{I}, k_j)$ of the keypoint k_j . Therefore $\theta_i \in [\alpha \cdot \phi(\mathcal{I}, k_j), \phi(\mathcal{I}, k_j)]$, with $\alpha \in [0, 1]$ being a system parameter of the generation method. Overall, N samples are drawn, so $i = 1, \dots, N$. The differences in the Boolean map generation are also visible in Fig. 1.

C. Attention Map Computation

The attention mechanism varies from the original BMS algorithm. Instead of defining surroundedness by masking regions connected to the borders in a Boolean map \mathcal{B}_i ,

we compute the activation map $\mathcal{M}(\mathcal{B}_i)$ by using a set of M sparse keypoints $K = \{k_j = (x_j, y_j) : j = 1, \dots, M\}$ to add context information. These keypoints can be drawn from human annotations (e. g., [2]) or from learned models. Importantly, for the studied use case, we define a keypoint such that it is always placed in a region of high interest and, therefore, with a high saliency value. If a region in the Boolean map is connected to one of the keypoints, it should therefore also be of interest. This fact is exploited by activating the Boolean map with the keypoints as seeds instead of the image’s borders. This process can be formulated by

$$\mathcal{M}(\mathcal{B}_i) = \bigcup_{j=1}^M \text{FLOOD}(\mathcal{B}_i, k_j). \quad (2)$$

The function $\text{FLOOD}(\mathcal{B}_i, k_j)$ applies a flood-fill algorithm to \mathcal{B}_i with seed k_j and, therefore, returns a map containing only regions connected to the seed. Therefore, less patches are activated in the example workflow in Fig. 1. Note that this formulation does not rely on the position of the salient regions within the image. Activated regions can be in contact with the image border. This is not true for the original BMS method, which relies on the assumption that the image borders themselves do not contain salient regions and that they are centrally placed, the so-called Center Surround Antagonism (CSA). However, in many applications, the CSA cannot be assumed, and rather the contrary case is interesting. For example, when detecting unknown objects, their location can

be everywhere in the image, and assuming a prior centered distribution reduces the expressiveness of the computed visual saliency. If the CSA can be assumed, an additional computation step can be performed to enhance the resulting activation maps by intersecting the activation map with the calculated BMS activation map $\mathcal{M}_{\text{BMS}}(\mathcal{B}_i)$:

$$\mathcal{M}_{\text{comb}}(\mathcal{B}_i) = \mathcal{M}_{\text{BMS}}(\mathcal{B}_i) \cap \mathcal{M}(\mathcal{B}_i). \quad (3)$$

For the following examples, we will only use the first definition from Equation (2) because the CSA cannot be assumed for the PVDN dataset [2]. Also, note that in contrast to the original BMS method, we do not split the activation maps into sub-activation maps $\mathcal{M}^+(\mathcal{B}_i)$ and $\mathcal{M}^-(\mathcal{B}_i)$. This has two reasons: First, for thresholds below the keypoint intensity, the keypoint will always have a value of 1.0 in the corresponding Boolean map \mathcal{B}_i and therefore $\mathcal{M}^-(\mathcal{B}_i)$ will mostly be empty. Second, for higher intensities, the keypoint is likely connected to large image regions, which causes “leakage” of the computed attention. Also, no dilation operation is performed on the activation map $\mathcal{M}(\mathcal{B}_i)$ since we found no real benefit for the studied application. Consequently, the attention map $\mathcal{A}(\mathcal{B}_i)$ is simply calculated by

$$\mathcal{A}(\mathcal{B}_i) = \frac{\mathcal{M}(\mathcal{B}_i)}{\|\mathcal{M}(\mathcal{B}_i)\|_2}. \quad (4)$$

As a final step, all attention maps are averaged into a mean attention map $\bar{\mathcal{A}}$ with

$$\bar{\mathcal{A}} = \frac{1}{N} \sum_{i=1}^N \mathcal{A}(\mathcal{B}_i), \quad (5)$$

as described by Zhang and Sclaroff [21]. If multiple keypoint classes exist, the steps above can be performed for each class separately, yielding one mean attention map per class. For example, this is used for the generation of attention maps for direct and indirect keypoint annotations of the PVDN dataset, as presented in the following.

IV. FURTHER APPLICATIONS

Beyond the studied application for the PVDN dataset, the proposed method can be applied to all areas where one wants to detect or annotate objects with fuzzy object boundaries. This is, for example, often the case with biological image data of fluorescence microscopy [22], [23], [24]. Depending on the signal-to-noise ratio, the localization and tracking of the fuzzy objects of interest (cells) pose a challenge so that the proposed saliency method is advantageous in this area as well.

V. EXPERIMENTS

As previously mentioned, the annotation via sparse keypoints in the PVDN dataset allows for automatically deriving various other object representations. With the following experiments, we want to demonstrate the versatility of the proposed saliency method for objectively creating bounding boxes as well as binary masks. Thus, we show that the problem of provident vehicle detection at night can be tackled from both the perspective of object detection as well as semantic segmentation.

A. Automatic Bounding Box Generation

Since it is common in object detection tasks to infer bounding boxes, a logical step is to generate bounding boxes for the dataset in order to use SOTA algorithms. For that, Saralajew et al. [2] already proposed an algorithm as well as a proper metric to measure the quality of the automatically generated boxes given the keypoint annotations. We show that by generating binary maps using visual saliency with the keypoints as fixation points, we can derive higher-quality bounding boxes than the previously proposed approach.

We shortly recap the proposed bounding box metric by Saralajew et al. [2]. The metric phrases the problem of detecting and classifying light instances of oncoming vehicles at night as an object detection problem with binary classification, meaning whether the object is a relevant light instance (direct or indirect) or it is not. The primary goal of this bounding box metric is to make predicted bounding boxes comparable with the ground-truth keypoints. It follows the idea that

- each bounding box should span around exactly one keypoint, and
- each keypoint should lie within exactly one bounding box.

The following detection events are introduced:

- True positive: The instance is described (at least one bounding box spans over the keypoint);
- False positive: The bounding box describes no instance (no keypoint lies within the bounding box);
- False negative: The instance is not described (no bounding box spans over the keypoint).

With that, precision, recall, and F-score can be computed in the usual manner. Additionally, in order to quantify the bounding box quality of true-positive events, the following quantities are defined:

- $n_K(b)$: The number of keypoints in a bounding box b that is a true positive;
- $n_B(k)$: The number of bounding boxes that are true positives and that cover a described keypoint k .

With that, the quality measures can be computed as

$$q_K = \frac{1}{N_B} \sum_b \frac{1}{n_K(b)}$$

and

$$q_B = \frac{1}{N_K} \sum_k \frac{1}{n_B(k)},$$

where N_B and N_K are the total number of true-positive bounding boxes and annotated keypoints, respectively. The overall quality is determined by $q = q_K \cdot q_B$.

Our bounding box generation pipeline consists of the following steps:

- 1) For each keypoint in an image, calculate the saliency map using the keypoint as the fixation point (see Section III).
- 2) Using a standard blob detection approach, we derive the bounding box coordinates of each saliency blob. In

some cases, this results in several overlapping bounding boxes.

- 3) For all possible combinations of bounding boxes derived from each keypoint annotation, we calculate the F-score and the bounding-box metric (as proposed by Saralajew et al. [2]). Our first decision criterion is the F-score since we want to capture as many keypoints as possible. Here, the recall can be used equivalently, as precision is always 1.0. This is caused by the fact that bounding boxes generated with our saliency method cannot be false positive since bounding boxes are only created if there is a keypoint annotated. The second decision criterion then is the bounding-box metric, since out of the combinations with the highest F-score we want to retrieve the one with the highest quality. As the metric is designed to penalize if several bounding boxes contain the same keypoints, choosing a combination with a high bounding-box metric value will lead to non-overlapping bounding boxes.

An example of these steps can be seen in Fig. 2. For each scene, we derive the optimal parameter setting for the saliency map generator by optimizing the product of the F-score and the bounding box metric using a Tree-structured Parzen Estimator approach. This can be considered as a standard hyperparameter tuning. *Thus, each scene has a specifically parameterized saliency map generator.* In the approach of Saralajew et al. [2], a general parameter setting for the bounding box generator was derived only based on the train split since in their approach, the bounding box generator was also part of the final model. However, in our case the bounding box generator is not part of the final prediction and classification model itself, which is why we can use specific parameter settings for each scene in order to obtain the best possible ground-truth bounding boxes for each scene.

The results of the proposed saliency-based bounding box generation approach are shown in Table I. With our method for generating bounding boxes based on the keypoint annotations, we clearly outperform the previous approaches both in terms of F-score and bounding box quality [25], [2]. However, when training the SOTA object detection algorithm YoloV5⁵ on the newly generated bounding boxes, we see that it cannot exploit the full potential of the ground truth. In terms of F-score, it is even inferior compared to the YoloV5 version trained based on the bounding boxes generated by the previously proposed methods. Nevertheless, with a bounding box quality score of 0.86, we see that the bounding boxes which are predicted correctly are of very high quality. Saralajew et al. [2] already supposed that YoloV5 was learning the heuristics of their blob detector which they used to generate the bounding boxes. Since they used the same parameter setting for all scenes, the blob detector can be considered an easy rule-based image processing algorithm with fairly low complexity and thus easily learnable for a SOTA object detection algorithm as YoloV5. Yet, in our case, we use a differently parameterized saliency map generator for each scene. For this reason, it is

difficult to learn a general representation of the bounding box generation algorithm, increasing the complexity of the task by far. Furthermore, by increasing the quality of the bounding boxes, the task inherently becomes more difficult. A high bounding box quality indicates that each keypoint has a single corresponding bounding box, and only a few bounding boxes span over multiple keypoints. Thus, the algorithm has to distinguish between neighboring light instances and cannot simply predict a larger bounding box spanning over several keypoint annotations. This explanation provides a rationale for why YoloV5 performs worse in terms of F-score although being trained on better ground-truth bounding boxes.

B. Semantic Segmentation of Relevant Light Instances

Saliency maps were extracted from the keypoint annotations, which can be used for a multitude of computer vision tasks. Besides the generation of bounding boxes, the saliency maps can also be used as ground truth for semantic segmentation. Thus, the task of provident vehicle detection at night can be converted from an object detection task to semantic segmentation of relevant light areas in the image. For this, the saliency maps are binarized and three labels are used as ground truth: direct light instances, indirect light instances, and background. As a proof of concept, we trained a fully convolutional encoder-decoder style network on the created saliency maps and evaluated the results.

Based on previous fully convolutional models [26], [27], [28], a ResNet50 [29] backbone was used to create low resolution feature maps. These were then upsampled to the input image resolution by five layers of transposed convolution. The model was trained using a learning rate of 10^{-4} for 20 epochs. For the evaluation of the model's prediction, two metrics were used: The mean Intersection over Union (mIoU), which is the standard metric for SOTA semantic segmentations, and a custom keypoint-based metric that takes the underlying keypoint annotations into consideration. The keypoint metric analyzes whether the predicted areas for direct and indirect light instances contain their respective ground-truth keypoints. For that, blobs of connected areas are extracted, and each blob is analyzed. Therefore, modifying the already described events for bounding boxes in Section V-A, the following events for semantic segmentation are introduced:

- True positive: A ground-truth keypoint's location is predicted to be of the correct label;
- False positive: A predicted light instance area does not contain any keypoint;
- False negative: A ground-truth keypoint's location is predicted to be of an incorrect label.

Using these events, precision, recall, and F-score can be calculated as usual. After evaluating the model on the test-split of the PVDN dataset, an mIoU of 0.55 was determined. The keypoint-based metric reached a precision of 0.79, a recall of 0.53, and an F-score of 0.64. These values appear mediocre at first. However, a deeper analysis of the network's predictions reveals more promising results: Fig. 3 shows two examples of predictions that are correct but result in very low IoUs. On the left, two reflections on the street are shown that

⁵<https://github.com/ultralytics/yolov5>

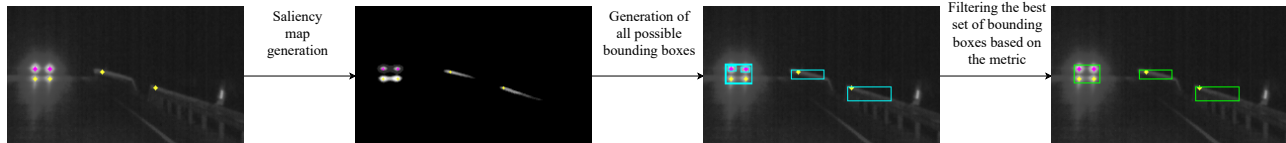


Fig. 2. Bounding box generation pipeline using Boolean map saliency and the ground-truth keypoints. The first image shows the original scene with the light instances annotated via keypoints (pink: direct, yellow: indirect). In the first step, the saliency map for each keypoint is generated. For better visualization, the image shows the cumulated saliency map for all keypoints. Then, for each saliency map, the bounding boxes are determined. Finally, the combination of bounding boxes yielding the highest F-score and highest bounding box metric is filtered and selected.

TABLE I
COMPARISON OF BOUNDING BOX GENERATION METHODS.

Model	Precision	Recall	F-score	q	q_K	q_B
Bounding Box Generation [2]	1.00	0.69	0.81	0.42	0.42 ± 0.24	1.00 ± 0.00
YoloV5x [2]	1.00	0.68	0.81	0.37	0.38 ± 0.20	0.98 ± 0.08
YoloV5s [2]	0.99	0.66	0.80	0.37	0.38 ± 0.20	0.98 ± 0.09
Bounding Box Generation [25]	1.00	0.87	0.93	0.70	0.70 ± 0.30	1.00 ± 0.00
Bounding Box Generation (ours)	1.00	0.88	0.94	0.86	0.86 ± 0.25	1.00 ± 0.00
YoloV5s (ours)	0.97	0.53	0.69	0.84	0.87 ± 0.24	0.99 ± 0.05
YoloV5x (ours)	0.97	0.58	0.73	0.86	0.87 ± 0.24	1.00 ± 0.04

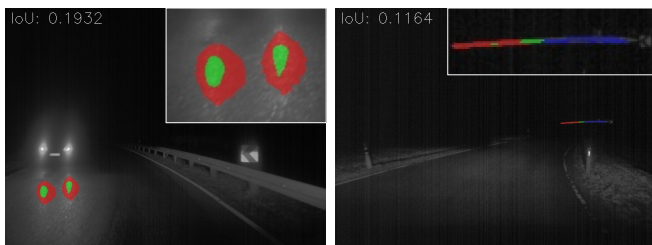


Fig. 3. Examples for low IoU on correct predictions of indirect instances. The red area annotates the ground truth, while the blue annotates the prediction. The intersection of ground truth and prediction is marked in green. On the upper left of each image, the found IoU for the indirect light instances is displayed.

are correctly detected by the model, as depicted by the green areas. However, this intersection area only covers small parts of the whole ground-truth area. Consequently, the resulting IoU only reaches around 19% although the detection is not incorrect. A similar case is shown on the right side: Both the ground truth in red and the model’s prediction in blue annotate the same reflecting guardrail. However, the prediction mostly covers the right side while the ground truth is located on the left of the guardrail, resulting in a small IoU of around 12% although the prediction contains the correct information, which is that there is an oncoming but not yet visible vehicle.

The IoU is a metric designed for objects with clear boundaries so that even slight deviations from the shape defined in the ground truth are measurable. With light reflections, we cannot guarantee clear boundaries and, moreover, for the use case studied in this paper, it is of less importance to capture the exact area described by the ground truth but rather the general region in which are light instances of oncoming vehicles. Consequently, the proposed keypoint metric is more

suited for this task because it is invariant to the shape as long as it covers a ground-truth keypoint. However, as the results show, the achieved performance with respect to this measure is also not optimal. By inspecting the prediction results, we can confirm that this is mainly due to the limits of the measure to model the invariance (keypoints are not correctly covered). Two examples for correct predictions—in the sense of the task to predict light reflections—which are counted as incorrect are shown in Fig. 4: On the left side, the predicted areas of two street reflections are shown. It can be seen that the left keypoint is not covered by the predicted area in blue, which therefore makes the keypoint a false negative, and the prediction above is a false positive. This increases the number of false-positive detections, although the prediction of the model can be considered correct. On the right side, the prediction on a guardrail is shown. Both the prediction and the ground-truth keypoint annotate the guardrail as a reflecting object, which should make this prediction a true positive. However, the prediction is scattered over three different parts of the guardrail, with the keypoint just not being covered by one of the predictions. Therefore, this intuitively correct prediction creates three false positives and one false negative count. Cases like these show that the keypoint metric is also not fully suited to describe the quality of the model’s prediction.

To show that the model’s predictions are in fact much better than the previous metrics indicate a third coarse metric was implemented. This metric aims at answering the question of whether the model predicts an approaching vehicle in a frame or not. The ground truth and the model’s prediction are therefore reduced to a binary classification for this metric, depending on whether a frame contains ground-truth keypoints and whether any pixel of the segmentation maps contain

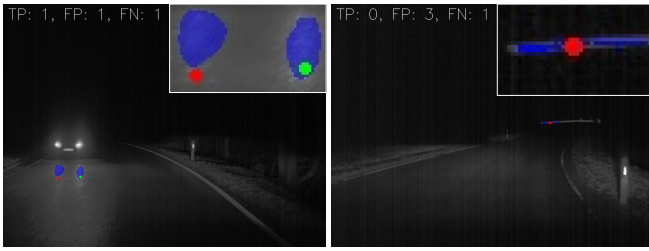


Fig. 4. Examples for correct predictions which just fall short of covering the ground-truth keypoint. The blue area marks the model’s prediction while red and green dots annotate the positions of ground-truth keypoints. Green keypoints are covered by the model’s prediction and are therefore true positives. Red keypoints are not covered and are therefore counted as false negatives. On the upper left of each image, the calculated scores for the indirect keypoints are displayed.

predictions of direct or indirect light. The resulting scores are calculated as follows:

- True Positive: Both ground truth and prediction contain the same information of whether a vehicle is oncoming or not;
- False Positive: The ground truth does not contain any annotated keypoints but the predicted segmentation maps include direct or indirect light pixels;
- False Negative: The ground truth contains annotated keypoints but the model does not predict any areas of direct or indirect light.

Again, using these scores, precision, recall, and F-score are calculated as usual. On the test split, a recall of 0.91 was reached, meaning that in 91 % of all frames an oncoming vehicle was correctly detected. A precision of 0.98 also shows that false-positive detections are very rare. In total, an F-score of 0.94 was reached.

We experimented with different parameters for the saliency map generation and found that the overall size of the used ground-truth saliency maps have an impact on the behavior of the model. If the neural network is trained on relatively small saliency maps, it focuses mostly on brighter light instances and sometimes does not detect reflections with low light intensity. The model, therefore, creates only a few false-positive detections, resulting in a high precision but a lower recall. When training on larger saliency maps, the neural network is forced to also create brighter and larger heatmaps for light instances. This causes smaller, less intense light instances to be detected more consistently but also makes the system more prone to false positives, resulting in a higher recall but less precision.

Every scene of the PVDN dataset contains multiple frames, which can be categorized as follows:

- Frames not containing any direct or indirect light;
- Frames containing *only* indirect light in the form of reflections in the environment;
- Frames which contain a directly visible vehicle.

We analyzed their distribution in the dataset and found that 7.4% of frames contain *only* indirect light while frames containing direct light make up 56.6% of the dataset. Due to this discrepancy, the automated saliency map optimization

focuses mostly on the frames with directly visible vehicles. As a result, some saliency maps in frames containing only indirect instances are very small and do not cover the full area of reflection. However, these frames are extremely important when detecting vehicles before they are directly visible. An example for such a suboptimal ground-truth saliency map is shown in Fig. 3 on the right. The ground-truth saliency map in red and green only covers the left part of the guardrail, although it is fully illuminated by the oncoming vehicle. A perfect ground-truth saliency map would cover the guardrail fully in this frame. As we already mentioned, larger ground-truth saliency maps can increase the recall of less intense light reflections. Separately optimizing the parameters for frames only containing indirect light instances could therefore improve the model’s performance on the provident detection of vehicles.

VI. CONCLUSION AND FUTURE WORK

Following up on the previous work of Saralajew et al. [2], we presented an approach to generate various object representations based on sparse keypoint annotations using visual saliency in order to detect oncoming vehicles at night before they are actually directly visible. We showed that when using our saliency approach, the task can easily be phrased both as an object detection as well as a semantic segmentation problem. The proposed approach is able to automatically generate high-quality bounding boxes based on the annotated keypoints describing the direct and indirect light artifacts. Although we derived better bounding boxes from the keypoint annotations than previous approaches, the experiments show that SOTA object detection methods have difficulties learning based on this. The reason might be that the proposed bounding box generation approach is much more complex than those of previous methods and, therefore, making it hard for algorithms to learn the underlying logic of generating the bounding boxes.

Furthermore, in a proof of concept, we showed that with our saliency method we can automatically generate binary masks for direct and indirect light instances. With this, we trained a neural network for semantic segmentation and proved that the task of providently detecting vehicles at night can also be solved as a semantic segmentation problem. However, current metrics for semantic segmentation such as mIoU do not fully account for the inherently fuzzy nature of light reflections. Consequently, we proposed a metric specifically designed for detecting oncoming vehicles at night before direct sight. Yet, we still see the need for further investigation of proper metrics to deal with fuzzy objects where spatial positions are not objectively definable and, moreover, where the basic underlying task allows such variations in the predictions. For example, in the case of provident vehicle detection at night, it is not always necessary to predict the exact location of a light reflection, since the final overall task is to predict where the vehicle will occur in the image, not where the light reflection is located. Consequently, such a metric should also be able to allow spatially volatile predictions to a certain extent. Additional to finding proper metrics to deal with

fuzzy objects in images, future work should concentrate on designing special algorithms for the task of detecting vehicles providently to efficiently use the few samples of indirect light instances present in the PVDN dataset. In the future, we plan to specifically address this problem.

In summary, in this paper, we provided further perspectives and tools that rely on visual saliency to tackle the problem of provident vehicle detection at night. At this point, we want to emphasize that although the methods are evaluated on the specific automotive use case, we are confident that they can be transferred to other domains where fuzzy and objectively non-definable object boundaries are present, such as biological image data of fluorescence microscopy.

REFERENCES

- [1] E. Oldenziel, L. Ohnemus, and S. Saralajew, "Provident detection of vehicles at night," in *2020 IEEE Intelligent Vehicles Symposium (IV)*, 2020, pp. 472–479.
- [2] S. Saralajew, L. Ohnemus, L. Ewecker, E. Asan, S. Isele, and S. Roos, "A dataset for provident vehicle detection at night," in *2021 IEEE/RSJ International Conference on Intelligent Robots and Systems (IROS)*. IEEE, 2021, pp. 9750–9757.
- [3] I. Ullah, M. Jian, S. Hussain, J. Guo, H. Yu, X. Wang, and Y. Yin, "A brief survey of visual saliency detection," *Multimedia Tools and Applications*, vol. 79, no. 45–46, pp. 34 605–34 645, apr 2020.
- [4] L. Itti, C. Koch, and E. Niebur, "A model of saliency-based visual attention for rapid scene analysis," *IEEE Transactions on Pattern Analysis and Machine Intelligence*, vol. 20, no. 11, pp. 1254–1259, 1998.
- [5] L. Itti and C. Koch, "Comparison of feature combination strategies for saliency-based visual attention systems," in *Human Vision and Electronic Imaging IV*, B. E. Rogowitz and T. N. Pappas, Eds. SPIE, may 1999.
- [6] J. Zhang and S. Sclaroff, "Saliency detection: A boolean map approach," in *2013 IEEE International Conference on Computer Vision*, 2013, pp. 153–160.
- [7] M. Jian, W. Zhang, H. Yu, C. Cui, X. Nie, H. Zhang, and Y. Yin, "Saliency detection based on directional patches extraction and principal local color contrast," *Journal of Visual Communication and Image Representation*, vol. 57, pp. 1–11, nov 2018.
- [8] J. Zhang, Y. Dai, and F. Porikli, "Deep salient object detection by integrating multi-level cues," in *2017 IEEE Winter Conference on Applications of Computer Vision (WACV)*. IEEE, mar 2017.
- [9] J. Pan, E. Sayrol, X. Giro-i Nieto, K. McGuinness, and N. E. O'Connor, "Shallow and deep convolutional networks for saliency prediction," in *Proceedings of the IEEE conference on computer vision and pattern recognition*, 2016, pp. 598–606.
- [10] A. Kroner, M. Senden, K. Driessens, and R. Goebel, "Contextual encoder–decoder network for visual saliency prediction," *Neural Networks*, vol. 129, pp. 261–270, sep 2020.
- [11] G. Li, Y. Xie, L. Lin, and Y. Yu, "Instance-level salient object segmentation," in *Proceedings of the IEEE Conference on Computer Vision and Pattern Recognition (CVPR)*, July 2017.
- [12] J. Maldonado and L. A. Giefer, "A comparison of bottom-up models for spatial saliency predictions in autonomous driving," *Sensors*, vol. 21, no. 20, p. 6825, oct 2021.
- [13] F. Lateef, M. Kas, and Y. Ruichek, "Saliency heat-map as visual attention for autonomous driving using generative adversarial network (GAN)," *IEEE Transactions on Intelligent Transportation Systems*, pp. 1–14, 2021.
- [14] N. Pugeault and R. Bowden, "How much of driving is preattentive?" *IEEE Transactions on Vehicular Technology*, vol. 64, no. 12, pp. 5424–5438, dec 2015.
- [15] A. López, J. Hilgenstock, A. Busse, R. Baldrich, F. Lumbreras, and J. Serrat, "Nighttime vehicle detection for intelligent headlight control," in *Advanced Concepts for Intelligent Vision Systems*, ser. Lecture notes in Computer Science, J. Blanc-Talon, S. Bourennane, W. Philips, D. Popescu, and P. Scheunders, Eds. Springer, 2008, pp. 113–124.
- [16] P. Alcantarilla, L. Bergasa, P. Jiménez, I. Parra, D. Fernández, M.A. Sotelo, and S.S. Mayoral, "Automatic lightbeam controller for driver assistance," *Machine Vision and Applications*, pp. 1–17, 2011.
- [17] S. Eum and H. G. Jung, "Enhancing light blob detection for intelligent headlight control using lane detection," *IEEE Transactions on Intelligent Transportation Systems*, vol. 14, no. 2, pp. 1003–1011, 2013.
- [18] D. Jurić and S. Lončarić, "A method for on-road night-time vehicle headlight detection and tracking," in *2014 International Conference on Connected Vehicles and Expo (ICCVEx)*, 2014, pp. 655–660.
- [19] P. Sevekar and S. B. Dhonde, "Nighttime vehicle detection for intelligent headlight control: A review," in *Proceedings of the 2016 2nd International Conference on Applied and Theoretical Computing and Communication Technology (iCATccT)*, 2016, pp. 188–190.
- [20] R. K. Sazoda and M. M. Trivedi, "Looking at vehicles in the night: Detection and dynamics of rear lights," *IEEE Transactions on Intelligent Transportation Systems*, vol. 20, no. 12, pp. 4297–4307, 2019.
- [21] J. Zhang and S. Sclaroff, "Exploiting surroundedness for saliency detection: a Boolean map approach," *IEEE Trans. Pattern Analysis and Machine Intelligence (TPAMI)*, 2015.
- [22] I. Smal, M. Loog, W. Niessen, and E. Meijering, "Quantitative comparison of spot detection methods in fluorescence microscopy," *IEEE Transactions on Medical Imaging*, vol. 29, no. 2, pp. 282–301, 2010.
- [23] A. C.-Y. Wu and S. A. Rifkin, "Aro: A machine learning approach to identifying single molecules and estimating classification error in fluorescence microscopy images," *BMC Bioinformatics*, vol. 16, no. 1, pp. 1–8, 2015.
- [24] S. Abousamra, S. Adar, N. Elia, and R. Shilkrot, "Localization and tracking in 4d fluorescence microscopy imagery," in *2018 IEEE Conference on Computer Vision and Pattern Recognition Workshops, CVPR Workshops 2018, Salt Lake City, UT, USA, June 18-22, 2018*. Computer Vision Foundation / IEEE Computer Society, 2018, pp. 2290–2298.
- [25] L. Ewecker, E. Asan, L. Ohnemus, and S. Saralajew, "Provident vehicle detection at night for advanced driver assistance systems," *arXiv preprint arXiv:2107.11302 [cs.CV]*, 2021.
- [26] J. Long, E. Shelhamer, and T. Darrell, "Fully convolutional networks for semantic segmentation," Nov. 2014.
- [27] V. Badrinarayanan, A. Kendall, and R. Cipolla, "Segnet: A deep convolutional encoder-decoder architecture for image segmentation," Nov. 2015.
- [28] B. Xiao, H. Wu, and Y. Wei, "Simple baselines for human pose estimation and tracking," Apr. 2018.
- [29] K. He, X. Zhang, S. Ren, and J. Sun, "Deep residual learning for image recognition," in *Proceedings of the IEEE conference on Computer Vision and Pattern Recognition (CVPR)*, 2016, pp. 770–778.